# SIMULATION OF BEAM-INDUCED PLASMA IN GAS FILLED CAVITIES

K. Yu*, Stony Brook University, Stony Brook, NY 11794, USA
R. Samulyak#, Stony Brook University, Stony Brook, NY 11794 and BNL, Upton, NY 11973, USA
A. Tollestrup, K. Yonehara, Fermilab, Batavia, IL 60510, USA
B. Freemire, Illinois Institute of Technology, Chicago, IL 60616, USA
M. Chung, UNIST, Ulsan, Korea

*Abstract*

Understanding of the interaction of muon beams with plasma in muon cooling devices is important for the optimization of the muon cooling process. SPACE, a 3D electromagnetic particle-in-cell (EM-PIC) code, is used for the simulation support of the experimental program on the hydrogen gas filled RF cavity in the Mucool Test Area (MTA) at Fermilab. We have investigated the plasma dynamics in the RF cavity including the process of power dump by plasma (plasma loading), recombination of plasma, and plasma interaction with dopant material. By comparison with experiments in the MTA, simulations suggest several unknown properties of plasma such as the effective recombination rate, the electron attachment time on dopant molecule, and the ion – ion recombination rate in the plasma.

## INTRODUCTION

When a beam passes through a dense hydrogen gas filled RF (HPRF) cavity, the beam energy ionizes the gas. The induced plasma gains energy from the RF electric field applied to cavity. This effect is called plasma loading. The induced plasma undergoes complicated recombination processes. If a small amount of dopant (molecular oxygen) is added to the hydrogen gas, plasma electrons attach to dopant molecules, creating negatively charges ions and causing ion-ion recombination processes. These processes have been studied by experiments at the MuCool Test Area at Fermilab [1,2,3]. Simulation study has been used to compare the experiment results with the mathematical model and uncover unknown or uncertain properties from the experiments. Even though the recombination rate, attachment time, and ion-ion recombination are measured in experiments, the range of measurements is restricted in narrow region. Benchmarked with experimental data, simulations suggest those rates for a large experimental range. To enable such simulations, new algorithms to resolve plasma chemistry and plasma loading have been developed and implemented in SPACE [4].

## ATOMIC PHYSICS IN GAS-FILLED CAVITY

### *Plasma Formation*

As an intense proton beam propagates in the HPRF cavity, it generates plasma by ionization due to collision of beam particles with neutral gas molecules [5,6]. When the cavity is filled with pure hydrogen gas, the plasma is formed by electrons and hydrogen ion clusters. If dopant such as oxygen is added in the gas, electrons quickly attach to dopant molecules, creating negative ions [5,7]. The formation of plasma follows the beam shape because plasma particles are generated along beam particle trajectories, and the plasma particles cannot move far away from their initial position due to collisions with the dense neutral gas. The plasma column preserves its form as time evolves (Fig. 7), even though the density of plasma changes by successive beam injections and atomic processes such as electron ion recombination, electron attachment, and ion-ion recombination in the cavity.

### *Plasma Loading*

The energy loss by one plasma pair during one RF cycle, $dw$, is introduced [1,3] based on the electron or ion drift velocity ($v$) or mobility ($\mu$), and the external RF field ($E_0 \sin(\omega t)$):

$$dw = \mathrm{q} \int_0^T (v_e + v_+ + v_-)\, E_0 \sin(\omega t)\, dt$$
$$= \mathrm{q} \int_0^T (\mu_e + \mu_+ + \mu_-)\, {E_0}^2 \sin^2(\omega t)\, dt \quad (1)$$

where subscripts "e", "+", and "-" denote electron, positive ion (hydrogen), negative ion (oxygen), respectively, and T and $E_0$ are the period and peak magnitude of the RF cycle. The external electric field $E_0$ in Eq. (1) has spatial distribution related to the geometry of the cavity [3]. Even though $E_0$ is not constant in space, we can assume it is constant for each specific plasma pair during one RF cycle since plasma charges cannot move far away from their initial positions. But different plasma pair in different position may have different $E_0$. Spatial distribution of $E_0$ is implemented in the SPACE code. Analytic computation of Eq. (1) was compared with experiments in [1,2,5]. Numerical simulation results are compared with experiments in Fig. 2.

The power delivered to gas in cavity by plasma loading is given by

$$\mathrm{P} = \frac{(V_{peak} - V)V}{R} - CV\frac{dV}{dt} \quad (2)$$

where R, C, and $V_{peak}$ denote the shunt impedance, capacity of the cavity, and the peak RF voltage, respectively [1,3]. In simulations, the total power is computed and $E_0$ ($V$ in Eq. (2)) is updated at every time step. Functions implementing the electron drift velocity

* kwangmin.yu@stonybrook.edu
# rosamu@bnl.gov


ISBN 978-3-95450-168-7

from [8] and ion mobility from [2] are used in the SPACE code to compute $dw$ [Eq. (1)].

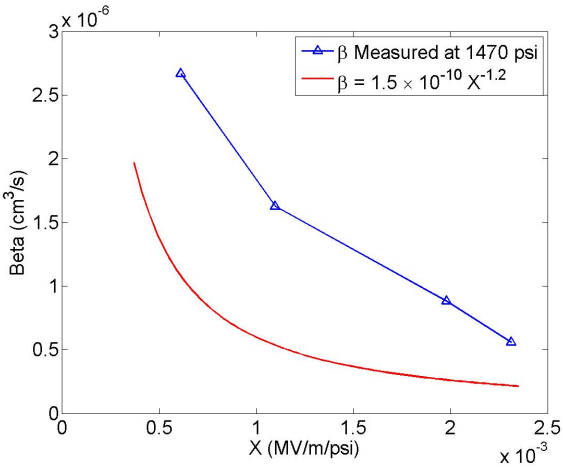


Figure 1: The effective recombination rate (Red curve) in the simulation which is chosen based on experimental measurement at 1470 psi. Simulations results in Fig. 2, 3, and 4 are obtained by using the red curve.

### *Electron-Ion Recombination*

When the cavity is filled with pure hydrogen gas, electrons and larger hydrogen clusters such as $H_3^+$, $H_5^+$, ⋯ compose the plasma [2,5]. In the process of recombination of electrons with positive ions, different hydrogen ions clusters have different recombination rates. The number of electrons is governed by the ionization and recombination rates as follows [5]:

$$\frac{dn_e}{dt} = N - \sum \beta_{H_m^+} n_e n_{H_m^+} \qquad (3)$$

where n with subscript, $\beta$ with subscript, and N denote number density of charges, electron-ion recombination rate with each hydrogen ion cluster, and the plasma generation rate. Even though the recombination rates are measured using a variety of methods, values of the recombination rates for larger clusters contain significant uncertainties, as well as the component ratio of hydrogen ion clusters. Thus the effective recombination is measured in the cavity. Using the effective recombination rate $\beta$, Eq. (3) can be written as follows:

$$\frac{dn_e}{dt} = N - \beta n_e \sum n_{H_m^+} \qquad (4)$$

The SPACE simulation of the HPRF cavity with the gas pressure of 100 atm (1470 psi) was compared with experimental results. There are four measurement of the recombination rate in the cavity under 1470 psi pressure. The electric field intensity rage of the measurement is restricted because it was measured in the equilibrium status [2].

The comparison of simulations with experiments provides data for computing recombination rates in a wide range of the electric field. With the effective recombination $\beta = 1.5 \times 10^{-10} X^{-1.2}$, where $X$ is $E/P$ (MV/m/psi) [Fig. 1], the simulation shows good agreement with experimental results. The difference between computed and measured values of the recombination rate is within measurement error range.

The process can be described as follows. After the start of the proton beam, the plasma generation rate by the beam ionization is faster compared to the recombination rate.

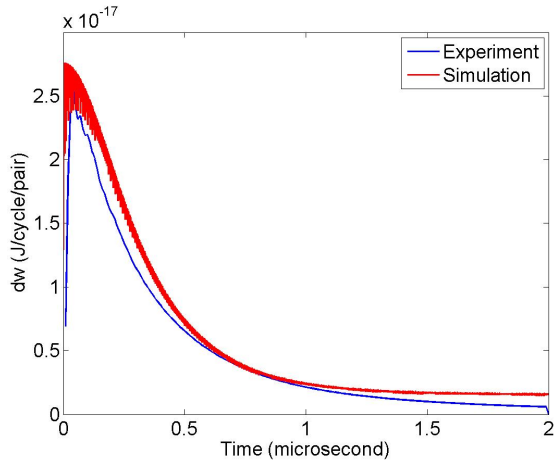


Figure 2: $dw$ comparison with experiment in 1470 psi.

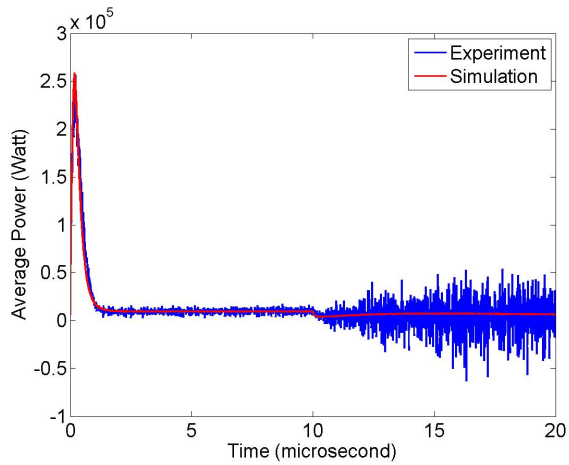


Figure 3: Power dissipation by the plasma comparison with experiment in 1470 psi.

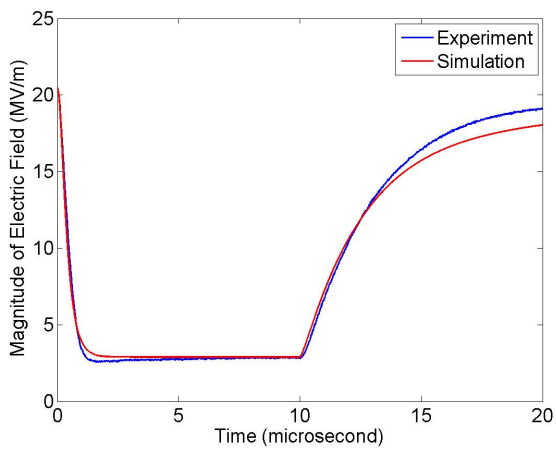


Figure 4: Electric field magnitude by plasma loading: comparison of experimental and simulation results in 1470 psi cavity.

By the plasma loading, the magnitude of RF field decreases and it reaches the equilibrium state when the plasma generation rate becomes in balance with

recombination. The equilibrium state starts at about 1 $\mu s$ in the 1470 psi experiment. The effective recombination rate is measured in the equilibrium [2]. After the proton beam leaves the cavity at 10 $\mu s$, only recombination takes place and the magnitude of the RF field is recovered [Fig. 3,4].

### *Attachment and Ion-Ion Recombination*

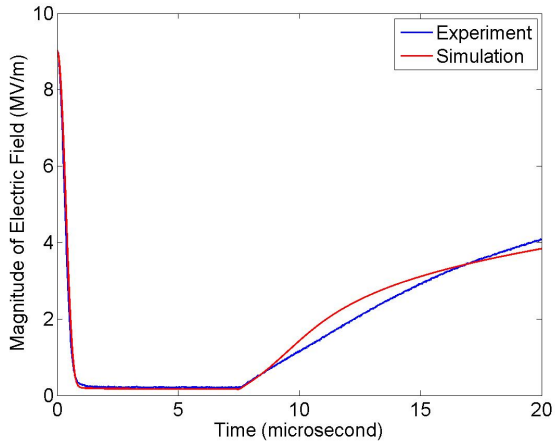


Figure. 5: Time evolution of electric field magnitude by plasma loading with $\beta = 1.5 \times 10^{-10}\, X^{-1.0}$. Comparison of experimental and simulation results in 300 psi pure hydrogen.

In the presence of the oxygen dopant, electrons recombine more quickly by attachment, the process that mitigates the plasma loading. Instead of Eq. (3), the following equations describe atomic processes in the cavity:

$$\frac{dn_e}{dt} = N - \beta_e\, n_e n_{H^+} - \frac{n_e}{\tau} \quad (5)$$

$$\frac{dn_{H^+}}{dt} = N - \beta_e\, n_e n_{H^+} - \eta\, n_{H^+} n_{O_2^-} \quad (6)$$

$$\frac{dn_{O_2^-}}{dt} = \frac{n_e}{\tau} - \eta\, n_{H^+} n_{O_2^-} \quad (7)$$

where $\tau$, $\eta$, $n_{H^+}$, and $n_{O_2^-}$ denote the attachment time, ion-ion recombination, and total hydrogen ion density including all clusters, and negative ion from dopant, respectively [2,7]. Based on experimental measurements, the simulations tested several attachment times and ion-ion recombination rates as function of $X$ ($E/P$ (MV/m/psi)). In the dopant case, the simulation is compared with the experiment in the cavity of 300 psi. Using the recombination value $\beta = 1.5 \times 10^{-10}\, X^{-1.0}$, calculated from the simulation of 300 psi pure hydrogen gas [Ref. Fig. 5], we performed simulations of 300 psi hydrogen doped with 1% dry air, and approximated the attachment time as $\tau = 4.0 \times 10^{-4}\, X^{2.5}$ and the ion-ion recombination rate as $\eta = 1.0 \times 10^{-10}\, X^{-1.0}$. Figure 6 shows the simulation result and comparison with the experiment.

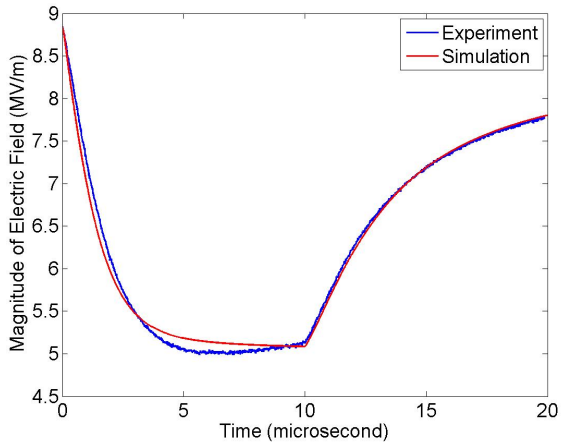


Figure 6: Electric field magnitude by plasma loading: comparison of experimental and simulation results in 300 psi cavity containing 1% dry air doped gas.

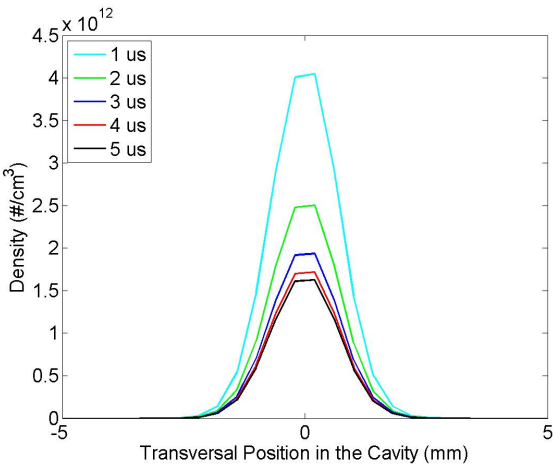


Figure 7: Electron density change in time of high density beam in 300 psi doped with 1% dry air.

## ACKNOWLEDGEMENT

The research was supported in part by the DOE Muon Accelerator Program.

## REFERENCES

[1] M. Chung et al, PRL 111, 184802 (2013).
[2] B. Freemire, Doctoral Thesis at IIT, 2013.
[3] K. Yonehara et al., Proceedings of IPAC 2013, TUPFI059.
[4] K. Yu et al., Proceedings of IPAC 2015, MOPMN012.
[5] B. Freemire et al., Proceedings of IPAC 2013, TUPFI064.
[6] K. Yu et al., Proceedings of IPAC 2014, MOPME043.
[7] B. Freemire et al., Proceedings of IPAC 2014, THPRI064.
[8] J.J. Lowke, Aust. J. Phys. 16, 115 (1962).




ISBN 978-3-95450-168-7